Remote optogenetic control of the enteric nervous system and brain-gut axis in freely-behaving mice enabled by a wireless, battery-free optoelectronic device

Andrew I. Efimov [a,b,1], Timothy J. Hibberd [c,1], Yue Wang [a,b], Mingzheng Wu [a], Kaiqing Zhang [d,e], Kaila Ting [a,f], Surabhi Madhvapathy [a,g], Min-Kyu Lee [a], Joohee Kim [a,h], Jiheon Kang [a], Mohammad Riahi [i], Haohui Zhang [d], Lee Travis [c], Emily J. Govier [c], Lianye Yang [l], Nigel Kelly [l], Yonggang Huang [a,d,g,j], Abraham Vázquez-Guardado [a,i,k,*], Nick J. Spencer [c,**], John A. Rogers [a,b,g,j,m,n,***]

[a] Querrey Simpson Institute for Bioelectronics, Northwestern University, Evanston, IL, 60208, USA
[b] Department of Biomedical Engineering, Northwestern University, Evanston, IL, 60208, USA
[c] College of Medicine and Public Health, Flinders Health and Medical Research Institute, Flinders University, Australia
[d] Department of Civil and Environmental Engineering, Northwestern University, Evanston, IL, 60208, USA
[e] State Key Laboratory of Structural Analysis, Optimization and CAE Software for Industrial Equipment, Department of Engineering Mechanics, Dalian University of Technology, Dalian, 116024, Liaoning, China
[f] Department of Neurobiology, Northwestern University, Evanston, IL, 60208, USA
[g] Department of Materials Science and Engineering, Northwestern University, Evanston, IL, 60208, USA
[h] Center for Bionics of Biomedical Research Division, Korea Institute of Science and Technology, Seoul, 02792, Republic of Korea
[i] Department of Electrical and Computer Engineering, North Carolina State University, Raleigh, NC, 27606, USA
[j] Department of Mechanical Engineering, Northwestern University, Evanston, IL, 60208, USA
[k] Center for Advanced Self-Powered Systems of Integrated Sensors and Technologies (ASSIST), North Carolina State University, Raleigh, NC, 27606, USA
[l] Department of Biomedical Engineering, Flinders Medical Centre, Bedford Park, South Australia, Australia
[m] Department of Neurological Surgery, Feinberg School of Medicine, Northwestern University, Chicago, IL, 60611, USA
[n] Center for Bio-Integrated Electronics, Northwestern University, Evanston, IL, 60208, USA

ARTICLE INFO

ABSTRACT

Wireless activation of the enteric nervous system (ENS) in freely moving animals with implantable optogenetic devices offers a unique and exciting opportunity to selectively control gastrointestinal (GI) transit *in vivo*, including the gut-brain axis. Programmed delivery of light to targeted locations in the GI-tract, however, poses many challenges not encountered within the central nervous system (CNS). We report here the development of a fully implantable, battery-free wireless device specifically designed for optogenetic control of the GI-tract, capable of generating sufficient light over large areas to robustly activate the ENS, potently inducing colonic motility *ex vivo* and increased propulsion *in vivo*. Use in *in vivo* studies reveals unique stimulation patterns that increase expulsion of colonic content, likely mediated in part by activation of an extrinsic brain-gut motor pathway, via pelvic nerves. This technology overcomes major limitations of conventional wireless optogenetic hardware designed for the CNS, providing targeted control of specific neurochemical classes of neurons in the ENS and brain-gut axis, for direct modulation of GI-transit and associated behaviours in freely moving animals.

* Corresponding author. Department of Electrical and Computer Engineering, North Carolina State University, Raleigh, NC, 27606, USA.
** Corresponding author.
*** Corresponding author. College of Medicine and Public Health, Flinders Health and Medical Research Institute, Flinders University, Australia.
  E-mail addresses: abraham.vg@ncsu.edu (A. Vázquez-Guardado), nicholas.spencer@flinders.edu.au (N.J. Spencer), jrogers@northwestern.edu (J.A. Rogers).
  [1] These authors contributed equally to this work.

1. Introduction

Increasing attention in recent years on the gut-brain axis is motivated by its critical role in diverse disease conditions (Margolis et al., 2021; Morais et al., 2021). For example, disorders of GI motility that lead to impaired transit of ingested content, prompt attempts to exert artificial control of the gut-brain axis to alleviate symptoms. Significant challenges exist, however, in selective manipulation of activity of neurons in the ENS and/or the neural pathways that link the gut to the brain in conscious, free-to-move animals. Current approaches, such as nonspecific electrical stimulation of peripheral nerves carry significant drawbacks, that include indiscriminate activation of both sensory and motor axons (Gao et al., 2021; Velasco-Benitez et al., 2023). Drugs similarly suffer from a broad spectrum of confounding effects as they act across multiple organ systems (Israelyan et al., 2019).

Due to remarkable levels of spatial, temporal, and cell-type specificity, optogenetic stimulation via implantable wireless optoelectronic devices offers significant promise as a method for developing therapies aimed at enhancing GI motility, *in vivo*. Existing wireless technologies for optogenetic control of the brain and spinal cord, however, are unsuitable for stimulation of the GI tract. Specifically, device requirements for use in the GI tract create major engineering challenges not present with non-contractile tissues like the brain and spinal cord. Unlike the CNS, the intrinsic neurons within the ENS lie between two independent layers of smooth muscle (Furness, 2012; Spencer and Hu, 2020). Thus, activation of enteric neurons requires deep light penetration, and the devices must operate reliably in the context of significant movements within the abdominal cavity, generated by gut smooth muscle. Designs must allow robust attachment to the gut wall *in vivo* during intense muscle contractions, but without inducing bowel obstruction and with the ability to optimize stimulus protocols and locations along the GI-tract for induction of GI-transit.

Here, we demonstrate a platform based on multiple light emitting diodes (LEDs) that overcomes limitations of related technologies designed for the CNS. The device takes the form of a fully implantable, wireless battery-free system capable of control over GI-motility and transit with user-defined stimulation parameters. This technology provides sufficient light intensity across large spatial fields, to reliably activate the ENS *ex vivo* and *in vivo*, without obstructing colonic transit, whilst remaining attached to the gut wall. The resulting targeted delivery of light to the colon can potently induce colonic motility *ex vivo* and increase transit *in vivo*. Enabled studies uncover a major excitatory brain-gut extrinsic pathway, involving pelvic motor neurons, that potently induces colonic transit and increased expulsion of content. More generally, the device technology introduced here has the potential to create significant, unique opportunities for targeted wireless control of the ENS and gut-brain axis in conscious, freely-moving animals.

2. Methods

2.1. Animals

Choline acetyltransferase (ChAT) cre mice (Strain #:006410) obtained from Dr. Marlene Hao at Melbourne University, were bred to a Rosa-CAG-LSL-ChR2(H134R)-eYFP-WPRE (Ai32) line and following cre-lox recombination, a colony of ChAT-ChR2^{Cre+} progeny was formed expressing the light sensitive ChannelRhodopsin-2 (ChR2) and the enhanced yellow fluorescent protein (eYFP) reporter in cholinergic neurons. Mice of either sex, from 1 to 6 months old, were housed in the Flinders Medical Center Animal Facility, under a 12-h light/dark cycle with food and water ad libitum.

2.2. Tissue preparation

Mice were euthanised by isoflurane overdose through inhalation and then exsanguinated, with approval from Flinders University, Animal Welfare Committee (ethics no. 4004). A midline laparotomy was performed, and the whole colon, mesentery and surrounding neurovascular tissue was removed. The tissue was placed in a Sylgard-lined glass Petri dish filled with room temperature or ice-cold Krebs solution (118 mM NaCl, 4.7 mM KCl, 1.0 mM NaH$_2$PO$_4$, 25 mM NaHCO$_3$, 1.2 mM MgCl$_2$, 11 mM D-glucose, 2.5 mM CaCl$_2$; bubbled with 95% O$_2$–5% CO$_2$). Luminal contents of the colon were flushed using a syringe with Krebs solution at 34–35 °C.

2.3. Mechanical recordings

A 2.5 mm stainless steel rod was inserted through the lumen of ChAT-ChR2^{Cre+} whole colons then mounted in an organ bath positioned on a water heater. Oxygenated Krebs solution at 35 °C perfused through the bath at a rate of ~5 mL/min 3–4 hooks through the muscularis externa of the colon, evenly spaced from the proximal to the distal end, recorded mechanical activity of the circular muscle underlying colonic motor complexes (CMCs). The hooks connected to custom-made isometric force transducers by suture thread with a basal resting tension of 0.5–1.0 g. The transducers fed to custom-made preamplifiers (Biomedical Engineering, Flinders University) connecting to a PowerLab 16/35 data acquisition unit (ADInstruments, Castle Hill, NSW, Australia), using LabChart 8 software (ADInstruments) on a Macintosh (iMac) computer for force recordings.

2.4. Ex vivo stimulation of isolated colon

One blue LED (Cree C479 DA2432, Three Five Materials, Inc.) was soldered to a printed circuit board and attached to 20 mm of enamelled copper wire, coated in Loctite 3554 light-cute acrylic and poly(dimethylsiloxane) (PDMS, Sylgard). A custom wired LED driver (Flinders Biomedical Engineering; BME1627) with a 0–15 V DC supply allowed manual control over the operation of the LEDs. A power line connected via the rear of the box supplied 10 V to the LEDs from the analogue output of an AD Instruments 16/35 Power Lab unit with a programmable pulse per millisecond sequence for each stimulation. Light intensity in mW/mm^2 as a function of applied voltage was characterized for 8 different LEDs used in these experiments, to account for slight variances in LED performance. Thresholds were tested on tissue, with maximum intensity used for experimental stimulations. Light outputs from single LEDs ranged from 0 to 45 mW/mm^2 from a corresponding applied voltage range from 2 to 15 V, respectively.

2.5. Ex vivo stimulation of brain-gut cholinergic rectal nerves

The full-length whole colon was removed from ChAT-ChR2^{Cre+} mice with extrinsic neural continuity retained to pelvic ganglia. The colon tube preparation was then pinned to a silicone-lined (Sylgard 184) organ bath at the proximal and distal extremities over an intraluminal stainless-steel rod. The mesentery and surrounding neural tissue were pinned to the silicone in a manner that exposed the rectal nerves between the prevertebral ganglia and mesentery. While recording mechanical activity, a single hard-wired blue LED was lowered onto the rectal nerves.

2.6. Device design and fabrication process

Assembly of the wireless battery-free device began with a custom flexible printed circuit board (fPCB; PCBWay) consisting of two layers of copper (18 μm) divided by a layer of polyimide (PI) (25 μm) with a PI coverlay (12.5 μm) over the PCB traces, as the base. A separate fPCB with the same layer stackup formed the paddle. Following component soldering, attachment of tinsel wires (type 1#, Roundteck Intl. Co.) used a through-hole solder connection on both ends for added strength. These wires, which offer relatively high strength (1.0 kgf) and resistance to mechanical fatigue, consist of a thin helical copper winding around a

polyester core, with a total thickness of 0.70 mm. The three LEDs (0.99 × 0.99 mm^2, Cree SA1000 450 nm) solder to the paddle extensions of the devices. An ultra violet (UV) curable adhesive (Norland 61; NOA61) formed a layer over the components and exposed solder joint regions of the fPCB to strengthen device component attachment. A 10 μm thick layer of parylene-C (10 μm), applied by vapor deposition, formed a biocompatible barrier to biofluids. A layer of PDMS coated on both sides of the two fPCBs created a soft interface between the device and surrounding tissue (Fig. 1A). Finally, silicone sealant (Kwik-Sil) at the interfaces between the interconnects and the fPCB further insulated the wires from bending fatigue, as shown in Fig. S1.

2.7. Electronic control and user interface

Graphical user interface software, designed and implemented in MATLAB (The MathWorks, Inc.), provides with remote control over individual devices using near field communication (NFC) protocols. The wireless devices utilize an 8-bit microcontroller (ATtiny84, Atmel) and an NFC read-write random access memory chip (M24LR04E, STMicroelectronics) as the basis of control and bidirectional wireless communication (Yang et al., 2021). This system integration enables real-time read and write capabilities to program illumination parameters such as the frequency, pulse width, inter pulse delay, and number of LEDs. Fig. 1E shows the block diagram of operation. The LEDs operate sequentially, one after the other with the programmed pulsed width and frequency. For example, a 20 Hz frequency (50 ms) illumination protocol allows for pulse widths of no more than 16 ms.

2.8. Optoelectronic characterization

Experimental measurements quantify the maximum optical power (OP) delivered at the target site by the LEDs (C470-SA1000, Cree) during wireless operation. Current delivered to the LED was measured with an ammeter in a cage enclosure with radio frequency (RF) power supplied to the external antenna in the range of 2 W and 10 W, the latter for studies reported here. Wires from the LED to the ammeter were twisted and oriented vertically within the cage to minimize interference with the RF. In separate measurements, an integrating sphere photodiode power sensor (S140C, Thorlabs) yielded the OP output as a function of current supplied to an individual LED during wired operation.

2.9. Optical simulations

The Monte Carlo simulation method captures the optical propagation and volumetric illumination profiles in the colon tissue (Wang et al., 1995). The total numerical volume is (8 mm)^3 distributed in 400^3 bins, each with an individual volume of (20 μm)^3. The model uses a simplified geometry in the form of a hollow cylinder of 2.7 mm diameter with 0.25 mm walls filled with aqueous media and surrounded by fatty tissue (Fig. S2). This model represents a colon largely empty of solid material. In a second model the hollow cylinder has a diameter of 1.35 mm to simulate a contracted colon. The absorption (μ$_a$) and scattering (μ$_s$) coefficients and the anisotropy factor (g) for the materials are as follows: colon tissue (μ$_a$ = 1.31 cm^{-1}, μ$_s$ = 221 cm^{-1}, g = 0.92) (Wei, 2005), fat tissue (μ$_a$ = 2 cm^{-1}, μ$_s$ = 150 cm^{-1}, g = 0.88) (Jacques, 2013; Michels et al., 2008) and water (μ$_a$ = 0.0001 cm^{-1}, μ$_s$ = 1 cm^{-1}, g = 0.9) (Pope and Fry, 1997). A blue LED (470 nm), located underneath the distal colon emits 7.05 mW of power, simulated as 9.96 × 10^6 photons emitted within a 120° full divergence angle over a squared surface area of the LED (0.99 × 0.99 mm^2). The optical flux is normalized to the irradiance at the surface of the LED (7.2 mW/mm^2). The illumination volume is calculated by integrating numerical bins with the colon tissue, not the aqueous nor the outside environment, whose irradiance is above the reference threshold (>1 mW/mm^2). A duplicate simulation, for both colon models, and volume analysis were performed for a μ-ILED (470 nm, 0.24 × 0.22 mm^2) that provides 1 mW of optical power, 19 mW/mm^2 irradiance at the surface.

2.10. Thermal simulations

Finite element models capture the thermal effects of the LEDs on adjacent tissue, due to heating from the LEDs and photothermal effects on a simulation volume that is shown in Fig. S2. Each LED produces 13.41 mW of thermal power and 7.05 mW of optical power. The simulation captures the illumination dynamics that correspond to continuous and phasic stimulation as described in Fig. S3. The transient-state thermal propagation considers the thermal power of the LEDs and the body heat flux caused by the optical fluence rate, and is controlled by the following governing equation (Yang et al., 2021):

$$\begin{cases} \rho C_p \dfrac{\partial T}{\partial t} + \nabla \bullet (-k\nabla T) = Q_{the} + \varphi\mu_a & \text{in } \Omega \\[2mm] \quad\quad\quad T = T_\infty & \text{on } \partial\Omega \end{cases}$$

Here, T is the temperature. ρ is the mass density, C_p is the heat capacity, and k is the thermal conductivity. Q_{the} is the heat source generated by the thermal power of multi-LED. φ is the optical fluence rate calculated in the optical simulation (Fang and Boas, 2009). Ω is the model region. Abaqus software was utilized for solving the governing equation by the finite element method. Linear tetrahedral element is used, and the minimum edge length is 100 μm. The thermal conductivity, heat capacity, and mass density of the materials used in the simulations are summarized in Table S1. The reported temperature increase in Fig. 2G corresponds to the volume of 990 × 990 × 250 μm^3 above the surface of the LED. The simulations captured the heat dissipation within the first 1 min. Beyond that, we employed a biexponential model, fitted to the simulation data ($1.09 - 0.42 \exp(-0.027t) - 0.34 \exp(-0.203t)$), to estimate the temperature increase at 4 min. The reported data in Fig. 2H corresponds to the temperature in the colon tissue along the z direction at the centre of the middle LED in the paddle.

2.11. Surgical implantation of wireless devices in vivo

All surgical procedures were approved by the Animal Welfare Committee of Flinders University (ethics approvals #4004), and all protocols were carried out in accordance with the National Health and Medical Research Council (NHMRC) Australian code for the care and use of animal for scientific purposes (8th edition, 2013) and recommendations from the NHMRC Guidelines to promote the wellbeing of animals used for scientific purposes (2008). ChAT-ChR2^{Cre+} Ai32 mice of either sex were anaesthetised with isoflurane; induced at 4% and then maintained at 1.5–2% in 1 L/min oxygen. The depth of anaesthesia was monitored by lack of response to a hind limb or tail pinch. Upon failure to elicit a tail or hind limb pinch, a midline laparotomy was made to expose the abdominal cavity. Mice were positioned on a thermostat-controlled heat mat to maintain body temperature throughout device implantation (Adloheat, Pakenham, Vic, Australia). Before incision, animals were administered s.c. 0.05 mg/kg buprenorphine (Temvet). The dorsal surface was shaved and cleaned with 0.5% chlorhexidine and 70% alcohol swab (Briemar). A laparotomy was performed, and the LED paddle was positioned under the pelvic bone with LEDs facing the rectum. The device receiver was positioned subcutaneously proximal to the LED paddle with wiring fed through the abdominal muscle. Post recording, the mouse was euthanised and LED positioning relative to the rectum was inspected to verify its location.

2.12. Propulsion of colonic content

ChAT-ChR2^{Cre+} mouse colon with pellets (natural faecal contents) remaining were placed in Sylgard-lined organ bath with oxygenated Krebs solution perfused at 35 °C. The colon was stimulated with a wireless blue LED at the proximal-mid or distal region. A dino-lite digital

microscope camera was set up directly above preparations to record propulsive movements of the natural faecal contents before, during and after stimulation. ImageJ (v1.53a, NIH) was used to measure the distance of the pellet movements.

2.13. Immunohistochemistry

The colon of C57BJ/6 mice and ChAT-ChR2^{Cre+} mice were cut along the mesenteric border, then stretched and pinned to a Sylgard-lined Petri dish to create a flat sheet. The tissue was then fixed using 4% paraformaldehyde for approximately 12 h and after, was washed in phosphate buffer solution (PBS). The mucosa and submucosa were removed and then sections of the tissue were cut from the proximal, mid, and distal colon. Tissue was immersed in 0.5% triton in PBS then blocked with 10% normal horse serum (NHS) in antibody diluent, and then incubated for 48 h in 1:2000 anti-ChAT rabbit (Schemann) and 1:2000 anti-NOS sheep (Emson) diluted with 10% NHS (Gibco) in antibody diluent. The tissue was cleared with PBS and incubated in 1:200 Cy3 donkey anti-rabbit and Cy5 donkey anti-sheep with antibody diluent for 12 h. Tissue was then washed in PBS and mounted onto microscopy slides with 100% glycerol.

2.14. Image capture and fluorescence microscopy

The slides were viewed under a fluorescence microscope filters (IX71; Olympus) with fluorophores FITC, Cy3 and Cy5 (Chroma Technology) with a Å~20 objective water-immersion lens. A Rodger scientific (Coolsnap) camera along with AnalySIS Imager 5.0 (SIS; Olympus, Münster, Germany) was used to capture micrographs of myenteric ganglia in FITC, Cy3 and Cy5 filters, that were saved as TIFF files.

2.15. Analysis of behavioural movements

Voluntary movements of mice prior to, during and after optogenetic stimulation were capture using a Marshall compact HD camera product #CV346 at 30 frames/s. Data was analysed using Ethovision video tracking software (Noldus).

2.16. Quantification of colocalization

The colocalization of the eYFP marker in cholinergic neurons and NOS positive neurons was quantified by overlaying images of myenteric ganglia in the three different fluorophore filters using ImageJ (v1.53a, NIH) (Schneider et al., 2012).

2.17. Statistics and analysis

A mixed-effects model with a Tukey multiple comparison test was used to confirm colocalization of eYFP in ChAT and NOS positive neurons. LabChart 8 software was used to quantify CMC amplitudes and intervals of spontaneous and evoked CMCs. Intervals were defined by the point at which 50% on the rising phase of a single CMC was compared to the same point on the peak of the next proceeding CMC. Statistical analysis was performed using Prism 10 (GraphPad Software, Inc. La Jolla, CA, USA). Spontaneous intervals were compared to the intervals preceding evoked CMCs with either mixed-effects model or a two-way ANOVA and corrected for multiple pairwise comparison using Tukey, Šídák, or Dunnett post-tests. Student's t-test was used for two-group comparisons and Chi-squared or Fisher's exact test was used in the analysis of contingency tables. The use of n in the results section refers to the number of animals (*in vivo*) or colons (*ex vivo*) on which observations were made.

3. Results

3.1. Engineering features of the device

Attempts to use standard wireless, implantable optical stimulators, originally designed for use on the spinal cord (Neurolux Inc.), on isolated colon from ChAT-ChR2^{Cre+} mice (see Methods) revealed a need for technologies specifically optimized for the GI-tract. These standard devices utilize a passive electronic circuit consisting of an inductive planar coil antenna, rectifier, and one microscale LED (μ-ILED; 220×240 μm^2). The antenna supports wireless power transfer through mechanisms of magnetic inductive coupling to a resonant antenna that surrounds the animal enclosure and receives power from an RF source that operates at the Industrial, Scientific and Medical radio band (ISM, 13.56 MHz). Modulating power supplied to this RF source serves as the basis for wireless control over the temporal operation of the μ-ILED. Using these devices at typical low duty cycles (20% duty cycle: 20 Hz, 10 ms pulses, 10 s trains) for optogenetics stimulation of *ex vivo* whole colon from ChAT-ChR2^{Cre+} mice led to contractile responses of the musculature in only 13 of 20 trials (n = 5) and only over partial length of colon (colonic motor complexes, CMCs), even at maximum operating power (12 W from the RF source). Further, surgical implantation onto the colon *in vivo* induced colonic obstructions in 12 of 20 mice tested.

These limitations motivated three essential engineering modifications to the electronic circuits and operating scheme, described in detail in the Methods section. First, a set of three large LEDs (0.99×0.99 mm^2) actuated in linear sequence replaces the single μ-ILED, as a strategy to increase the spatial field of illumination (Fig. 1A and B). These LEDs mount on a fixed paddle structure (LED paddle) with dimensions that allow insertion under the pelvic bone during implantation (Fig. 1C–D, Figs. S4A–C). Second, the addition of a microcontroller and a near field communication (NFC) chip allows for active user-programmable operation of these LEDs through standardized NFC protocols (ISO 15693, Fig. 1E), while the RF source operates in a continuous, non-modulated fashion (Yang et al., 2021). Third, these modifications, and the use of a low equivalent series resistance (ESR <0.01 Ω) ceramic capacitor bank (5×22 μF), allow the storage of energy (1.72 mJ at 5.6 V) harvested from the RF source continuously and between periods of LED activation (Ausra et al., 2021). For instance, in the specific examples presented here, the wireless device can drive a single LED with currents up to 7.65 mA at a voltage of 2.67 V (20.46 mW) under 10 W of input RF power to the source antenna (Fig. S5), which sets the maximum permissible power that the wireless device can provide. The operation of three LEDs simultaneously at this power level requires 61.3 mW, which is outside the capabilities of passive or active devices that operate in a synchronous modality. The sequential discharge of the capacitor bank described here, however, at times specified by the microcontroller (20% duty cycle: 20 Hz, 10 ms pulse widths, 5 ms pulse-pulse delay, 0.2 mJ per pulse), supplies constant power to each of the three LEDs providing illumination over a correspondingly larger area (3 mm × 1 mm) without affecting the stability of the microcontroller. These features form the basis for a fully implantable, wireless, battery-free optogenetic stimulator capable of delivering programmable illumination patterns at intensities commensurate with opsin activation thresholds and at areas sufficiently large for recruiting a significant population of neurons in the ENS (Fig. 1D).

The hardware architecture also involves key modifications. Here, one flexible printed circuit board (fPCB) serves as a base for the electronic components, referred to as the wireless receiver, and another separate fPCB, the paddle structure, supports the three LEDs, referred to as the LED paddle, (Fig. 1A and B). These fPCBs join via ultrathin, flexible tinsel wires (15 mm long and 0.22 mm diameter), as outlined in the Methods section. The base and paddle have dimensions of 11 mm × 14.75 mm (17 mm if including the optional suture tab) and 13.1 mm × 1.4 mm, respectively. The use of a remote station, in the form of a graphic user interface (GUI) in MATLAB, and microcontroller firmware
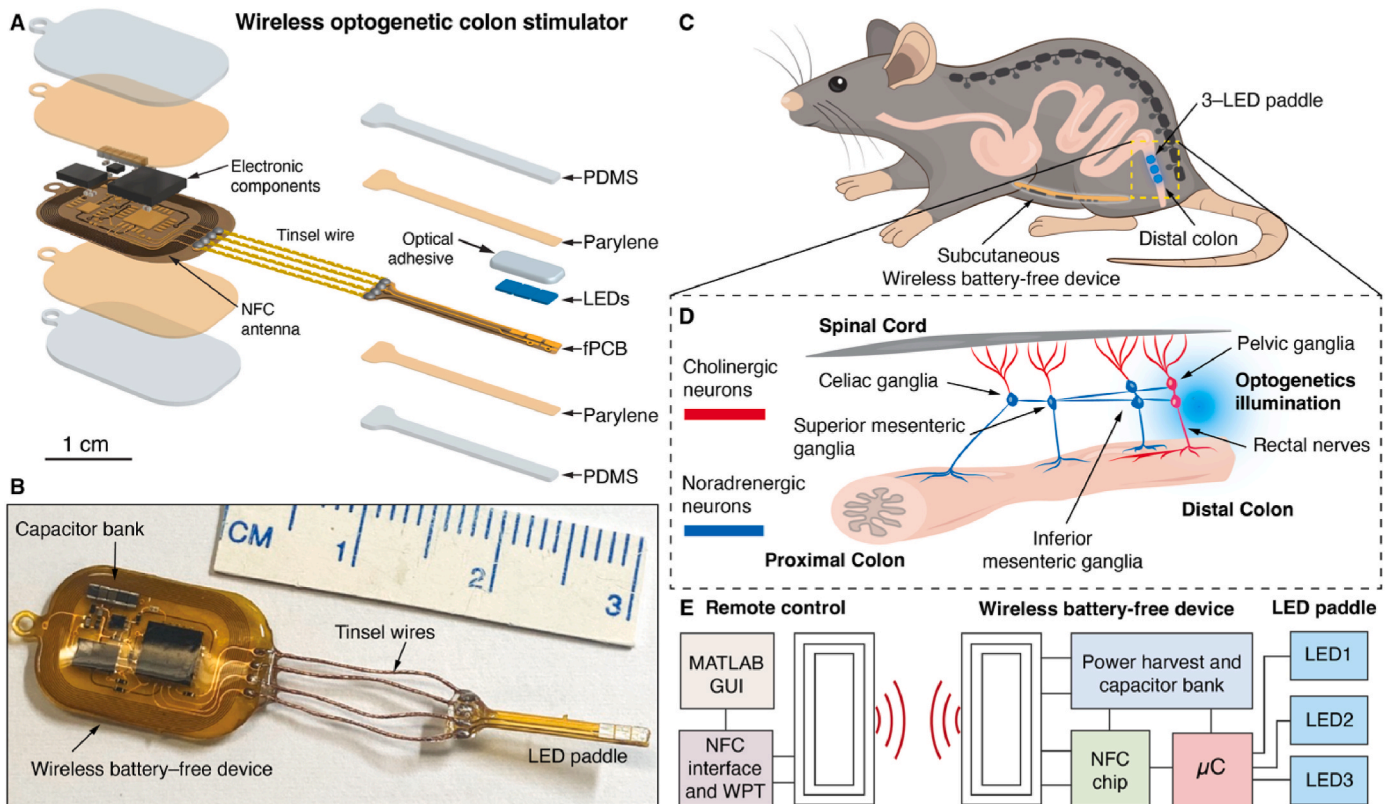
Fig. 1. Wireless implantable battery-free device for *in vivo* optogenetics stimulation of the colon. (**A**) Exploded-view diagram of the device that show the representative layers and components of the device. (**B**) Photograph of a fabricated device. (**C**) Diagrammatic representation of the location of the implanted receiver and paddle structure with LEDs in the terminal colon in a mouse. (**D**) Schematic illustration of the large intestine showing extrinsic cholinergic neural inputs from spinal cord (red), including post ganglionic cholinergic excitatory neurons in pelvic ganglia and their axons along rectal nerves (red). Inhibitory noradrenergic neurons/axons arising from sympathetic prevertebral ganglia are shown in blue. The rectal/pelvic nerves provide the major parasympathetic excitatory nerve pathway to the colon. (**E**) Block diagram of the functional modules associated with the wireless battery-free device and its interaction with the remote (MATLAB GUI) station.

provides real-time control to the operational parameters of the implanted device such as illumination activation, frequency and pulse widths, as described in the Methods.

Previously reported devices that incorporate serpentine interconnect structures and microfabricated features work effectively for CNS applications (Yang et al., 2021). However, they do not operate reliably in the gut due to mechanical failures of the metal features and/or the encapsulating layers induced by natural motions and muscle contractions within the gut. The wiring is critically important in this context. Requirements are both for sufficient strength to avoid fatigue during cyclic strains and for sufficient flexibility to eliminate constraints on natural movements. Among many candidate materials and wire designs, the tinsel type shown in Fig. 1B performs best in both benchtop testing and *in vivo* settings. Unlike single-stranded or multithreaded insulated wires, these tinsel interconnects survive ~200 cycles of manual bending (90° in all four directions, more aggressive than those expected in the animal; and soaking in 37 °C PBS solution) without failure. The strategic integration of these tinsel wires with the fPCBs is important to maintain structural robustness. A through-hole solder pad ensures mechanical strength at the solder joints where the interconnects meet the fPCBs (Fig. 1B). A UV curable epoxy (Norland Optical Adhesive 61) forms a protective structure on the top and bottom sides of the soldered tinsel wires. A conformal encapsulation layer of parylene-C (thickness ~10 μm) on both fPCB platforms and the wires serves as a barrier to biofluid penetration (Fig. 1A). To avoid fatigue at the location in Fig. S1A where failures can occur in the parylene-C layer, a silicone elastomer (Kwik-Sil) applied over the epoxy shifts the location of bending away from the interface between the solder and the epoxy, as in Figs. S1B–C.

3.2. Optical characteristics of the device

The use of large-area LEDs offers multiple benefits to achieve larger volume of illumination to the colon tissue. Monte Carlo models of light propagation in colon tissue capture the spatial distribution of illumination of the array of comparatively large LEDs used here (0.99×0.99 mm^2), compared to previously reported isolated μ-ILEDs (0.22×0.24 mm^2). The model places the illumination on the distal colon, represented by a tube with 2.7 mm diameter, and 0.25 mm in wall thickness, surrounded by adipose tissue, see Methods. The optical power provided by a single LED is 7.05 mW, or 7.2 mW/mm^2 irradiance at its surface. Considering the reference illumination threshold of 1 mW/mm^2 for ChR2 (Klapoetke et al., 2014), a single LED illuminates 0.43 mm^3 of colon tissue (Fig. 2A–C). The array of three LEDs, with centre-to-centre separations of 1 mm, reach up to 1.29 mm^3 total illuminated volume (Fig. 2C). In contrast, an individual μ-ILED that produces 1 mW optical power, or 19 mW/mm^2 at its surface, illuminates only 0.03 mm^3 for the same ChR2 activation threshold (Fig. 2C, Fig. S6A). Relative to this value, the illumination system reported here increases the illumination volume by 43 times (Fig. 2C). In other physiological conditions, i.e. when the colon is contracted (1.35 mm diameter), this illumination enhancement factor is 84 times (Fig. 2D, Figs. S6B–C).

3.3. Thermal characteristics of the device

The LEDs impose thermal loads that have the potential to affect living tissues. Numerical simulations that use the finite element method (FEM) account for heat production due to operation of the LEDs along with associated photothermal effects in the tissues for the specific
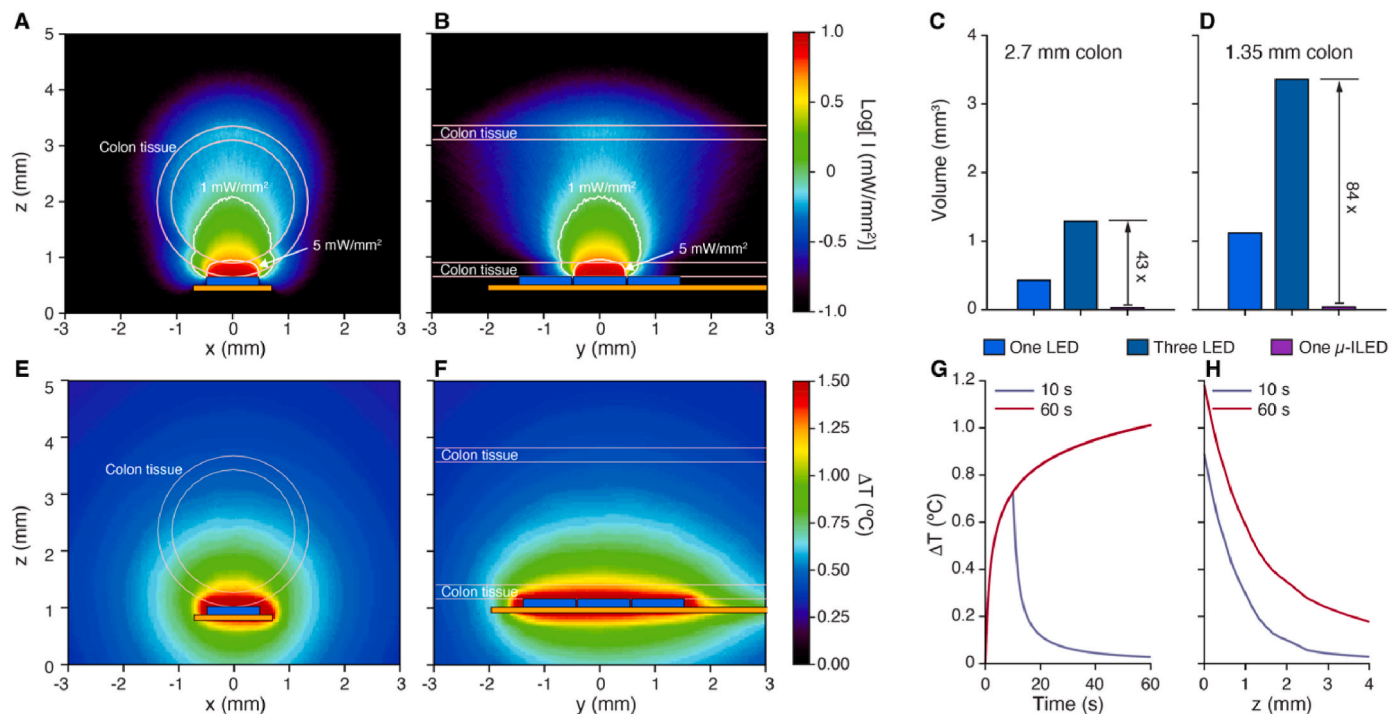
Fig. 2. Optical and thermal simulations demonstrate efficient light stimulation with safe thermal load for *in vivo* applications. (**A**) Transversal and (**B**) longitudinal cross-sectional views of the irradiance profile produced by one LED producing 7.05 mW of optical power (7.2 mW/mm^2). The white line represents the 5 mW/mm^2 (inner) and 1 mW/mm^2 (outer) irradiance contours. The former is used to calculate the illumination volume in the domain of the colon tissue. (**C**) Illumination volume produced by one LED and three LEDs (7.2 mW/mm^2 per LED) and its comparison with one μ-ILED (19 mW/mm^2) in the in domain defined by the colon tissue 2.7 mm diameter. (**D**) Same comparison as in C for a 1.35 mm diameter colon model. (**E**) Transversal and (**F**) longitudinal cross-sectional views of the heat distribution in the colon tissue after 60 s of optogenetic stimulation of three LEDs in sequential activation at 20 Hz, 10 ms pulse width (20% duty cycle). Each LED produces 13.41 mW of thermal power and 7.05 mW of optical power. (**G**) Transient temperature response in the colon tissue for two protocols of illumination: continuous and phasic (Fig. S3). (**H**) Heat propagation along the normal axis of the LED (z direction, z = 0 corresponds to the LED's surface) showing the heat penetration in the colon tissue.

systems used in this work, see Methods. Approximately 65% of the electrical power delivered to the LEDs is converted to heat (13.41 mW). The other 35% corresponds to the optical power (7.05 mW) delivered to the tissue. Monte Carlo simulations define the optical power absorbed in tissue, resulting in the photothermal effect. As an example, continuous stimulation (20 Hz, 10 ms pulse width, 20% duty cycle) such as those used in the *in vivo* validation (Fig. S3) increases the temperature in the adjacent colon tissue by 0.73 °C, 1.01 °C, and 1.09 °C above the body temperature after 10 s, 1 min, and 4 min of operation, respectively (Fig. 2E–G, Fig. S7). These values remain below thresholds for nociceptive sensations mediated by transient receptor potential (TRP) ion channels, such as Trpv1/v2, which specifically respond to temperatures exceeding the noxious range (>42 °C) (Patapoutian et al., 2003).

3.4. Ex vivo studies of cholinergic neurons in isolated colons

Initial tests examined the potential for blue light activation of cholinergic neurons to reliably evoke colonic motor responses in ChAT-ChR2^{Cre+} mice, via calibrated LEDs placed adjacent to *ex vivo* whole colons. These experiments involved repetitive stimuli (400 pulses, at 20 Hz, 10 ms pulse width, 20% duty cycle) applied to the proximal, mid, or distal regions of isolated whole colons. The results indicated that intensities ranging 10–25 mW/mm^2 readily elicit premature CMCs in all 20 ChAT-ChR2^{Cre+} mice tested (Fig. 3A and B). Evoked CMCs propagated along the full lengths of the isolated colons, with characteristics similar to those of spontaneous CMCs in amplitude (Fig. 3C) and without any sex-based differences in spontaneous or evoked CMC intervals or amplitudes (Fig. 3D and E). Stimulation of CMCs occurred at all tested locations along the colon, each of which typically resulted in CMCs originating from the stimulated location. In this respect, distal colonic

stimulation showed the highest fidelity with all distal stimulations evoking CMCs from the distal colon (Table 1). We tested the nicotinic receptor antagonist hexamethonium (100 μM) in 11 ChAT-ChR2^{Cre+} colons. As expected, hexamethonium blocked all spontaneous CMCs (Bush et al., 2000), while significantly smaller amplitude, non-propagating contractions could still be evoked at the site of blue light stimulation in 10 of 11 preparations (P < 0.001, main effect of hexamethonium, repeated measures 2-way ANOVA; hexamethonium n = 11, control n = 11). In 8 control mice that did not express ChR2, it was not possible to elicit any CMCs nor local contractions when the same stimulus parameters were applied to any regions along the colon. Importantly, nerve conduction blockade using tetrodotoxin (1 μM; n = 4) abolished all light-evoked contractions of the ChAT-ChR2^{Cre+} colon, confirming neural dependence. See Methods for experimental details.

3.5. Ex vivo induction of propulsion in isolated colons

Additional experiments were performed to examine the ability of the wireless battery-free device (Fig. 1) to induce propulsion in isolated ChAT-ChR2^{Cre+} colon. Whole colons containing endogenous fecal pellets were stimulated with light (4-min duration, 20 Hz frequency, 10 ms pulse width, 20% duty cycle) at either the proximal or distal regions using the wireless device. Stimulation of either region induces pellet movement (Fig. 3F–I). Movie 1 demonstrates wireless LED activation of the proximal colon leading to increased contractility along the full length of the isolated colon. Movie 2 shows wireless activation of the device following continuous stimulation from the distal colon, and an associated increase in aboral propulsion along the full length. Distal colonic stimulation induced greater distances of pellet propulsion when compared to pellet movements before or after stimulation (13.3 ± 6.0,
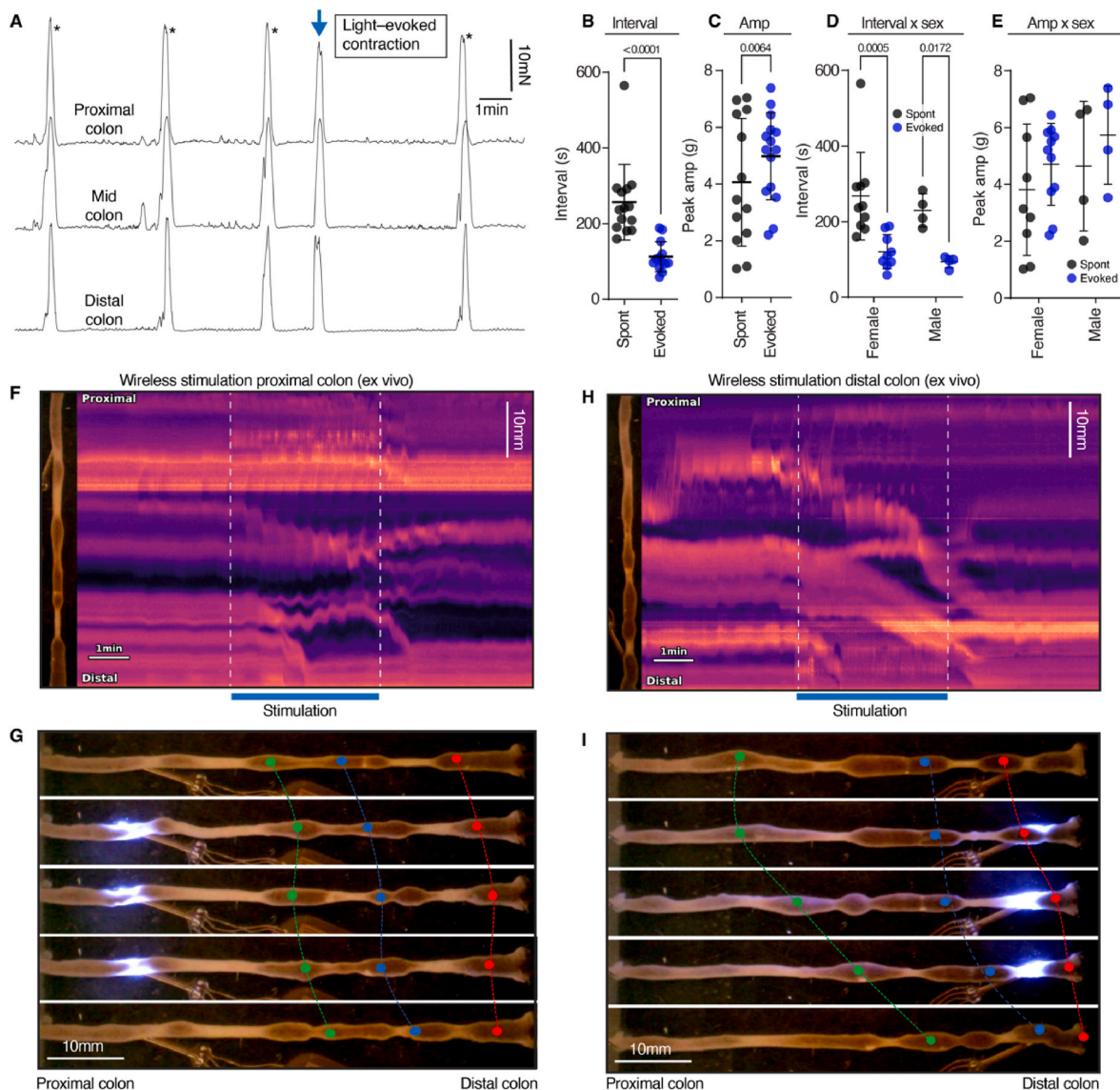
Fig. 3. Confirmation of light-evoked colonic motor complexes *ex vivo* in ChAT-ChR2^Cre+ mice. (**A**) Isometric force recording of spontaneous CMCs (see asterisk) and a premature, light-evoked, retrogradely propagating CMC (see arrow) in response to stimulation at 20 Hz for 10 ms and 400 pulses with 37 mW/mm^2. (**B**) Group analysis shows significant differences in intervals of prematurely evoked CMCs to light in *ex vivo* whole isolate colons. (**C**) Amplitudes of evoked and spontaneous CMCs were not different. (**D**) Intervals of light-evoked CMCs were not different between male and female mice. (**E**) Amplitudes of evoked and spontaneous CMCs to light were not different between male and female mice. A mixed-effects model corrected for multiple comparisons using Šídák's testing. (**F**) Spatio-temporal map of the effects of repetitive optogenetic wireless stimulation (20 Hz for 10 ms 400 pulses) of cholinergic neurons in the proximal region of isolated whole colon from ChAT-ChR2^Cre+ mice. The dynamic changes in light/dark shading represent changes in colon diameter along the length of proximal to distal colon. During the period of stimulation (between the dotted white lines) the short periods of lighter shading that span much of the length of colon represent brief contractions of the muscle (ie. gut diameter shortening) evoked by light. The darker shaded lines reflect dilations (widening) of the colonic wall. Contractions were evoked along the full length of colon with associated ejection of some pellets. (**G**) Images before, during, and after stimulation from the spatio-temporal map in **F**. This recording is shown in the real time Movie 1. (**H**) Spatio-temporal map showing the effects of distal colon stimulation using the same stimulus parameters as in **F**. Despite stimulation of the distal colon, evoked contractions propel fecal pellets distally along the length of colon where many were ejected. (**I**) Real time images from Movie 2 and the spatio-temporal map shown in **H**.

26.0 ± 27.4* 4.6 ± 4.7 mm movement before, during and after stimulation, respectively, *P = 0.0495 vs before; *P = 0.0051 vs after, Table 2, Dunnett's post-test, n = 4). In further experiments, similar *ex vivo* colon preparations were stimulated with a brief 10 s train at either proximal or distal colon (n = 16). Stimulations were defined as effective or ineffective based on pellet movement induced within the stimulation period. As suggested by the prior results, the distal colonic stimulations (14/16 effective trials) induced pellet propulsion significantly more effectively compared to proximal colonic stimulations (6/14 effective trials; P = 0.019; Fisher's exact test; n = 16).

3.6. In vivo stimulation of ChAT$^+$ neurons in the ENS and peripheral nerves

The wireless devices were implanted *in vivo,* positioned with the LEDs under the pelvic bone to deliver light directly to the distal colon and with the receiver located subcutaneously in the abdomen (Figs. S8A–B). The LED paddle slides 4–5 mm caudally under the pelvic bone to anchor the LEDs and prevent dislodgment from the colon, and to maintain direct illumination of the colonic surface (Fig. S8B). This design also provides access to a region of the distal colon known as a major target for potent control of the gut-brain axis, due to its high

Table 1
Light-evoked CMC origins relative to stimulation site (proximal, mid, or distal colon) *ex vivo*. Chi-squared test = 142, with adjusted standardized residuals >2 for each of proximal, mid, and distal stimulations and their matching origins, P < 0.001, total stimulation trials = 90, n = 13.

		CMC origin			
		Proximal	Mid	Distal	Total
Stimulus location	Proximal	25 *(89%)*	2 *(7%)*	1 *(4%)*	28
	Mid	4 *(13%)*	27 *(87%)*	0 *(0%)*	31
	Distal	0 *(0%)*	0 *(0%)*	31 *(100%)*	31
	Total	29	29	32	

Table 2
Pellet propulsion distance (mm) before, during and after optogenetic stimulation in colon, *ex vivo*.

	Pre	Stim	Post
Proximal colon	6.4 ± 8.8	10.3 ± 13.9	3.4 ± 4.7
Distal colon	13.3 ± 6.0	26.0 ± 27.4[a]	4.6 ± 4.7

[a] P = 0.0495 vs Pre; P = 0.0051 vs Post, Dunnett's post test.

innervation density (Spencer et al., 2014). The base resides subcutaneously on the lower abdomen, see Methods for detailed surgical procedure. Suturing the abdominal muscle tissue (Fig. S8C) followed by skin suturing (Fig. S8D) completes the surgery. 19 ChAT-ChR2^{Cre+} mice received a wireless device. In 15 of 19 animals, the LEDs remained adjacent to the colonic wall when inspected after experimentation, 4–5 days after implantation. In 4 of 19 mice, the LEDs were displaced from the space between the pelvic bone and colon, typically lying within the abdominal cavity.

To control known effects of environmental stress on colonic transit (Million et al., 2007), two stimulation protocols were applied to all mice on separate days (Fig. 4A). Protocol 1 involved 3 sequential 4-min periods: OFF, ON, OFF. Protocol 2 was reversed: ON, OFF, ON. Animals started on protocol 1 before protocol 2 or vice versa in equal numbers. In addition, two different stimulation paradigms were tested on all animals: continuous and phasic (Fig. S3) and these were compared with the following experimental controls: (1) ChAT-ChR2^{Cre+} mice implanted with a wireless device with inactive LEDs (device control) and (2) wild mice implanted with wireless devices with active LEDs (animal control). Continuous stimulation comprised ongoing stimulation (20% duty cycle; 10 ms pulse width, 20 Hz), as used *ex vivo*. Phasic stimulation comprised cycling between a 10 s stimulus train (20% duty cycle; 10 ms pulse width, 20 Hz) followed by 50 s quiescence. Thus, a 4-min phasic stimulation period comprised 4 stimulation-quiescence cycles.

Fig. S9 shows the pellet output patterns associated with each of the stimulation protocols *in vivo*. Only the phasic stimulation paradigm (Fig. 4B–D, Figs. S9A–B) increased pellet output, while the continuous stimulation paradigm (Fig. 4B–D, Figs. S9C–D) or experimental controls (animal and device controls) (Fig. 4B–D, Figs. S9E–F) showed no effect. In fact, phasic stimulation led to approximately twice as many fecal pellets (30 pellets) compared with non-stimulation periods (14 pellets) (Fig. 4D). The results across both protocols show that phasic stimulation during "ON" periods led to more pellet output than during "OFF" periods (P = 0.007 Šídák post-test, phasic stimulation n = 5; Fig. 4B–D), unlike continuous stimulation (P = 0.730, n = 5) or the experimental controls (P = 0.586, n = 5). This increase in colonic transit using phasic stimulation occured with no significant changes in the voluntary movements of the ChAT-ChR2^{Cre+} mice (P = 0.999 Šídák post-test, n = 5 phasic stimulation group, P = 0.112 Šídák post-test, n = 5 experimental control group; Fig. 4E-M).

3.7. Ex vivo studies of pelvic/rectal motor nerves activation of the brain-gut axis

Stimulation of extrinsic cholinergic axons (parasympathetic efferent neurons) in pelvic/rectal nerves is a mechanism by which wireless optogenetic stimulation of cholinergic neurons in the distal colon could increase colonic transit (Fig. 1D and 5A) (Furness, 1969). We rationalised that in our colony of ChAT-ChR2^{Cre+} mice, the peripheral cholinergic excitatory axons innervating the distal colon would express ChR2 arising from pelvic ganglia. Tests of the role of this brain-gut motor pathway used a preparation with the pelvic/rectal nerves attached to the isolated whole colon (Fig. 1D and 5A). This preparation involved delivery of pulses of blue light directly to the pelvic/rectal nerves *ex vivo*, whilst recording smooth muscle mechanical activity in the proximal, mid, and distal colon (Fig. 5B and C). Light stimulation of the pelvic/rectal nerves potently induced CMCs along the full length of isolated colon. CMC intervals with stimulation were significantly shorter compared to spontaneous intervals (control) (Fig. 5D–G), confirming CMCs were premature and thus evoked by the blue light stimulus. However, no stimulation effects were detected after severing the rectal nerves (n = 5), thus confirming the role of the rectal nerves and ruling out the possibility the effects were mediated by light diffusion onto the gut wall. The proportion of rectal nerve stimulations that evoked a CMC in the distal colon was 0.73 (n = 9), successfully stimulating propagating CMCs in 8 of 9 ChAT-ChR2^{Cre+} mice. Of the evoked CMCs in the distal colon, a proportion of 0.88 propagate retrogradely to the mid or proximal colon. Fig. 5B provides an example of a rectal nerve stimulation eliciting a retrogradely propagating CMC that is premature relative to the previous spontaneously occurring CMCs. Light-activated CMCs from pelvic/rectal nerve stimulation are significantly phase advanced, supported by significantly shorter intervals between spontaneous and light-evoked contractions (Fig. 5D and E). Light stimulation of the superior mesenteric nerves supplying the proximal colon, or lumbar colonic nerves to the distal colon did not evoke propagating CMCs (n = 4), showing selectively for the cholinergic pelvic nerve pathway.

3.8. Colocalization of eYFP in ChAT expressing neurons of the myenteric plexus

To determine the pattern of ChR2 expression in colon myenteric plexus, nerve cell bodies in ChAT-ChR2^{Cre+} mice (n = 4) and control C57B6/J mice (n = 4) were assessed for enhanced yellow fluorescent protein (eYFP) and immunoreactivity for choline acetyltransferase (ChAT) and nitric oxide synthase (NOS). Fluorescence of eYFP was only detected in ChAT-ChR2^{Cre+} colons (see Fig. 5H-M). The percentage of ChAT$^+$ neurons that contained eYFP was 90.8 ± 3.9% in the proximal colon, 89.5 ± 9.1% in the mid colon and 92.0 ± 3.4% in the distal colon. Conversely, the percentage of eYFP$^+$ neurons that were ChAT$^+$ is 96.0 ± 2.7%, 97.0 ± 1.4% and 93.3 ± 5.9% in the proximal, mid, and distal colon respectively. The percentage of eYFP$^+$ neurons that colocalised with both NOS and ChAT is 3.8 ± 0.6 to 5.3 ± 0.2% in all regions of the colon. Less than 1.4% of eYFP$^+$ neurons were NOS$^+$ but lacked ChAT. These values are represented graphically in Fig. S10.

4. Discussion

Studies of the intrinsic nervous system within the GI-tract can be greatly enhanced by the application of wireless optogenetic technology for selective control of gut motility and transit, including the gut-brain axis in free-to-move animals. The designs reported here overcome technical and anatomical challenges in developing gut-specific wireless LEDs that can remain attached to the gut wall *in vivo*, whilst also delivering illumination at sufficient intensities and over sufficient areas to activate the ENS, without inducing bowel obstruction. The resulting implantable wireless optogenetic technology can stimulate colonic motility and propulsion *ex vivo* and increase transit *in vivo*, whilst
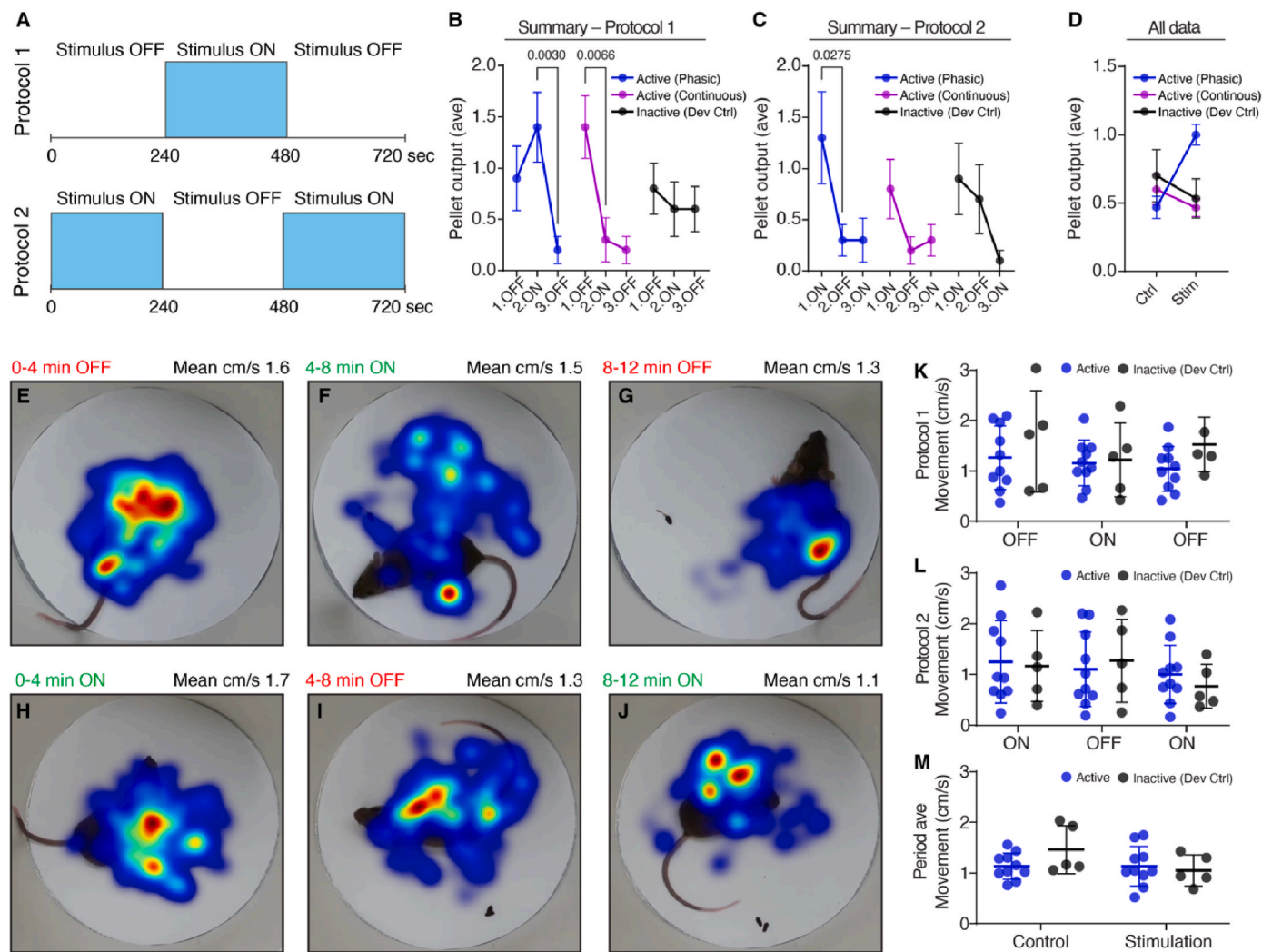
Fig. 4. Fecal pellet output over time in conscious free-to-move mice before, during, and after distal colonic wireless optogenetic stimulation using two stimulus protocols. (**A**) Graphical representation of the two protocols employed: Protocol 1 consists of a sequence of 4min/4min/4min where the stimulation is OFF/ON/OFF, respectively; Protocol 2 consists of a sequence of 4min/4min/4min where the stimulation is ON/OFF/ON, respectively. (**B**) Fecal pellet output results from Protocol 1 comparing phasic versus continuous stimulation and inactive (device control). Phasic, but not continuous stimulation or an inactive LED, showed increased pellet output when compared to the subsequent non-stimulation period (*P = 0.007, Šídák's post-test, n = 5). (**C**) Fecal pellet output results from Protocol 2 did not lead to increased pellet output. (**D**) Regardless of Protocols 1 or 2, inactive LEDs (device control) nor animal controls (control) did not show increased pellet output (P = 0.586). The use of Protocol 1 (**E–G**) or Protocol 2 (**H–J**) wireless optogenetic stimulation of ChAT$^+$ neurons in the enteric nervous system of freely-moving mice implanted with the device do not show changes in voluntary movement. (**K–M**) show quantification of animal movement. Neither Protocol 1 nor 2 led to significant changes in movement.

remaining in close contact to the gut. Typical materials used in implantable devices that stimulate the gastrointestinal tract are silicones, polymers (polyimide, parylene, styrene-ethylene-butylene-styrene thermoplastic elastomers), or even metallic casings, which serve the purpose to protect the electronics from biofluids, or as the substrates to carry the electrodes for stimulation (Kim, 2021). The device presented in this work employs materials such as polyimide substrate (the flexible printed circuit board; fPCB), parylene + silicone (PDMS) encapsulation which have been demonstrated to confer excellent biocompatibility in implantable devices (Reeder et al., 2022; Wu et al., 2022; Yang et al., 2021). In addition, these materials provide the device with a reliable biofluid barrier that prolongs its operation during chronic periods of implantation (Yang et al., 2021). Furthermore, one of the main advantages of this technology, however, is the miniaturized formfactor, highly functional battery free wireless optogenetic stimulator that allows the stimulation of soft tissue in freely behaving mice. The devices are well tolerated after *in vivo* surgical implantation throughout the duration of the experiment reported here: up to 8 days

(Fig. S4). No animals experienced bowel obstruction, infection, or welfare issues. An important additional aspect of these designs is that they rely only on commercially available components and standard assembly, thereby establishing pathways for scale-up and broad distribution.

Results obtained with this system indicate that specific patterns of wireless optogenetic stimulation of the distal colon are more selective than previous methods using electrical stimulation of the colon (Spencer and Bywater, 2002). In particular, optogenetic stimulation of pelvic cholinergic motor axons extrinsic to the colon lead to potent increases in fecal pellet output. The mechanism by which optogenetic activation of cholinergic axons (arising from pelvic ganglia) increases colonic motility and propulsion is due to the release of acetylcholine onto the myenteric plexus, from preganglionic cholinergic axons with cell bodies in pelvic plexus. Activation of these axons stimulates the enteric nervous system, leading to activation of muscarinic receptors on the smooth muscle causing muscle contraction. The propagation of CMCs along the colon in response to pelvic nerve stimulation is generated by activation of assemblies of ascending and descending interneurons that fire in repetitive
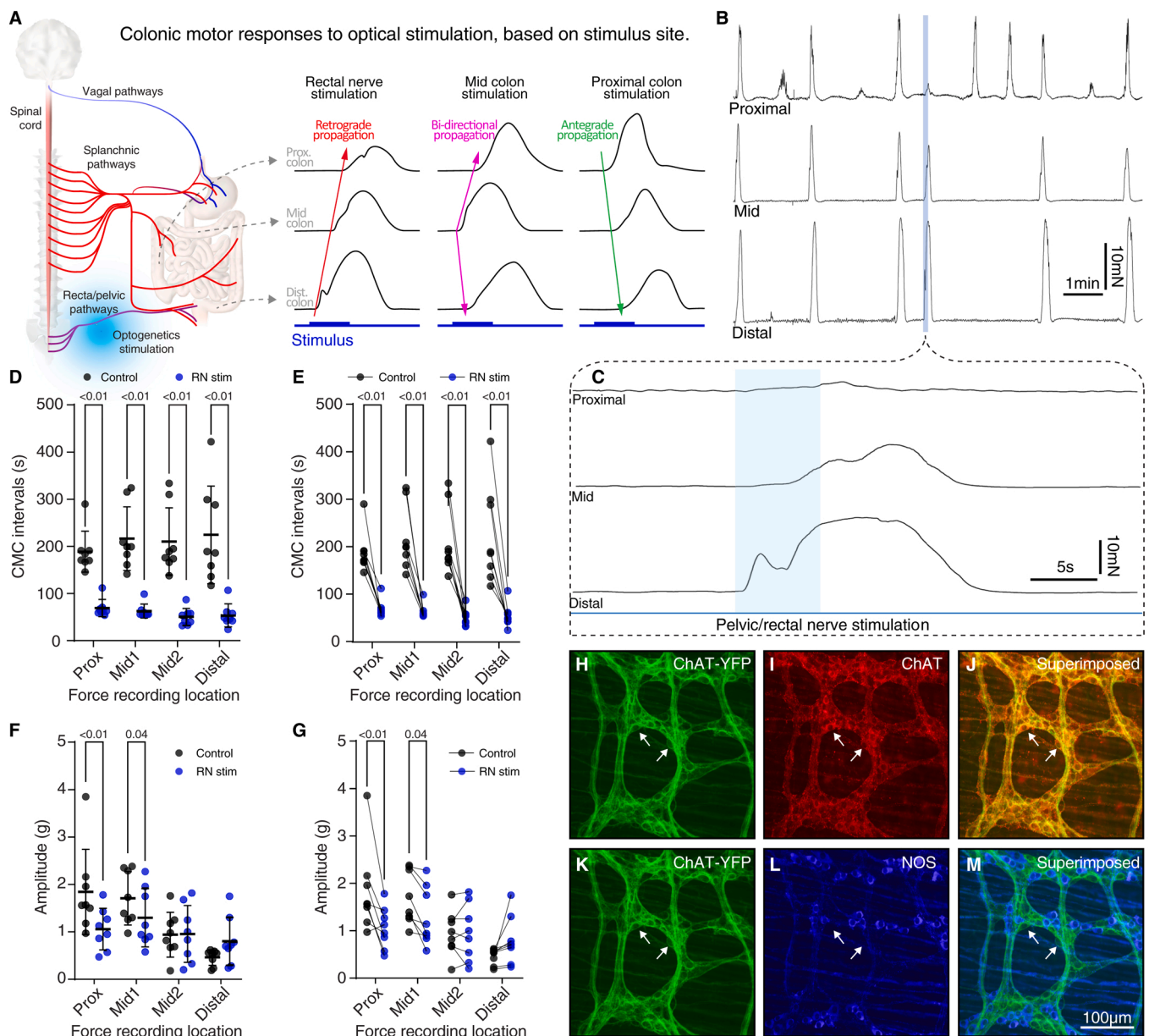
Fig. 5. Optogenetic stimulation of the brain-gut motor nerve pathway *ex vivo*. (**A**) Schematic diagram showing the site of optogenetic stimulation and the induced physiological effects. Left hand cartoon show location of optogenetic activation of pelvic/rectal nerves. Right hand images show the directionality of light-evoked contractions. Pelvic/rectal nerve stimulation evoked an orally propagating CMC contraction when no intraluminal content was present. Mid colon stimulation evoked a bidirectionally propagating CMC. Proximal colon stimulation can on occasion evoke an aborally propagating CMC contraction. (**B**) Isometric force recording, and (**C**) expanded scale, from circular muscle at three sites along the isolated whole colon showing the light-evoked CMC in response to stimulation of the pelvic/rectal motor nerves at 20 Hz for 10 ms and 200 pulses with 37 mW/mm². The blue marker indicates the onset of blue light delivered to the rectal nerves, which evoked a retrogradely propagating CMC contraction. (**D–E**) Mean CMC intervals (seconds) and (**F–G**) mean amplitudes between spontaneous CMCs (control) and CMCs evoked by rectal nerve stimulation (RN stim), n = 8. P-values displayed determined using 2-way ANOVA and Šídák's test for multiple comparison. (**H–M**) Micrographs showing nerve cell bodies in myenteric ganglia of ChAT-ChR2^Cre+ mouse colon confirming that ChAT-ChR2^Cre+ mice express ChR2 in the enteric nervous system. The fluorescence of eYFP, ChAT and NOS are shown in FITC, Cy3 and Cy5 filters respectively. (**J**) shows superimposed image of **H** & **I**, with colocalization of YFP with ChAT. The arrows in **H–J** indicate the same YFP+ neurons are ChAT+. In **K–M**, arrows indicate YFP+ neurons are not NOS+ (inhibitory) (**L**).

and coordinated bursts to generate CMCs (Spencer et al., 2018). Taken together, the findings suggest that selective optogenetic stimulation of cholinergic pelvic axons may be ideal therapeutic targets for on demand wireless control of colonic transit.

In humans, electrical stimulation of the sacral nerves can be effective in control of fecal incontinence, but many patients experience sensory disturbances during stimulation, likely due to indiscriminate activation of both sensory and motor axons along the pelvic/rectal nerves (Bielefeldt, 2016). The approaches reported here selectively stimulate excitatory motor axons optically within the pelvic-rectal nerves of the brain-gut axis, including the ENS of freely moving animals to increase colonic transit (Fig. 5A), without inducing behavioural stress or adverse nociceptive responses (Fig. 4E-M). Selective targeting of excitatory axons can markedly reduce the known off-target sensory effects of current commercially available neuromodulator devices that activate all axons between the gut and brain. Future devices could incorporate additional wavelengths of stimulating LEDs that are individually addressable to allow interaction with two or more distinct populations

of neurons on demand.

Whilst there are many benefits of using wireless implantable optogenetic technology to stimulate gastrointestinal motility *in vivo*, there are some drawbacks that are worth discussing, including the potential for infection, inflammation, or rejection of the foreign implantable body. Therefore, it is strongly advised that researchers perform preliminary pilot studies to optimize the surgical approaches, device preparation and implement the device validation during the intended period of use (Yang et al., 2022). Irrespective, there are major advantages of using targeted *on demand* optogenetic stimulation of specific neurochemical classes of axons within specific peripheral nerves to control colonic transit *in vivo*. Principally, we show that the method described here offers significant advantages in terms of spatio-temporal control of gut motility and transit, compared with current conventional non-specific therapeutic drugs that require oral absorption and act across multiple organ systems, with numerous unwanted side effects.

5. Conclusion

The findings show that specific stimulus regimens delivered with wireless optogenetic colon-specific devices can potently control activity within the ENS and gut-brain axis in freely-moving animals. Given the high prevalence of gastrointestinal motility disorders and the significant interest in gut-to-brain communication in health and disease, the technology described here can open major avenues for scientific enquiry that could lead in therapeutic solutions in the near future.

CRediT authorship contribution statement

Andrew I. Efimov: Writing – original draft, Visualization, Investigation, Formal analysis, Data curation. **Timothy J. Hibberd:** Writing – original draft, Visualization, Investigation, Formal analysis, Data curation. **Yue Wang:** Investigation. **Mingzheng Wu:** Investigation, Writing – review & editing. **Kaiqing Zhang:** Investigation. **Kaila Ting:** Investigation. **Surabhi Madhvapathy:** Investigation. **Min-Kyu Lee:** Investigation. **Joohee Kim:** Investigation. **Jiheon Kang:** Investigation. **Mohammad Riahi:** Visualization. **Haohui Zhang:** Investigation. **Lee Travis:** Investigation, Formal analysis. **Emily J. Govier:** Investigation, Formal analysis. **Lianye Yang:** Resources. **Nigel Kelly:** Resources. **Yonggang Huang:** Resources. **Abraham Vázquez-Guardado:** Writing – review & editing, Visualization, Software, Data curation. **Nick J. Spencer:** Writing – review & editing, Writing – original draft, Resources, Formal analysis, Data curation, Conceptualization. **John A. Rogers:** Writing – review & editing, Writing – original draft, Resources.

Declaration of competing interest

The authors declare the following financial interests/personal relationships which may be considered as potential competing interests: Nick J. Spencer reports financial support was provided by National Health and Medical Research Council (NHMRC). Nick J. Spencer reports financial support was provided by Australian Research Council (ARC) Discovery Project. Abraham Vázquez-Guardado reports financial support was provided by NC State University. John A. Rogers reports financial support was provided by Northwestern University Querrey Simpson Institute for Bioelectronics. If there are other authors, they declare that they have no known competing financial interests or personal relationships that could have appeared to influence the work reported in this paper.

Data availability

Data will be made available on request.

Appendix A. Supplementary data

Supplementary data to this article can be found online at https://doi.org/10.1016/j.bios.2024.116298.

References

Ausra, J., Wu, M., Zhang, X., Vázquez-Guardado, A., Skelton, P., Peralta, R., Avila, R., Murickan, T., Haney, C.R., Huang, Y., Rogers, J.A., Kozorovitskiy, Y., Gutruf, P., 2021. Wireless, battery-free, subdermally implantable platforms for transcranial and long-range optogenetics in freely moving animals. Proc. Natl. Acad. Sci. USA 118. https://doi.org/10.1073/pnas.2025775118.

Bielefeldt, K., 2016. Adverse events of sacral neuromodulation for fecal incontinence reported to the federal drug administration. World J. Gastrointest. Pharmacol. Therapeut 7, 294. https://doi.org/10.4292/wjgpt.v7.i2.294.

Bush, T.G., Spencer, N.J., Watters, N., Sanders, K.M., Smith, T.K., 2000. Spontaneous migrating motor complexes occur in both the terminal ileum and colon of the C57BL/6 mouse in vitro. Auton. Neurosci. 84, 162–168. https://doi.org/10.1016/S1566-0702(00)00201-0.

Fang, Q., Boas, D.A., 2009. Monte Carlo simulation of photon migration in 3D turbid media accelerated by graphics processing units. Opt Express 17, 20178. https://doi.org/10.1364/OE.17.020178.

Furness, J.B., 2012. The enteric nervous system and neurogastroenterology. Nat. Rev. Gastroenterol. Hepatol. 9, 286–294. https://doi.org/10.1038/nrgastro.2012.32.

Furness, J.B., 1969. An electrophysiological study of the innervation of the smooth muscle of the colon. J. Physiol. 205, 549–562. https://doi.org/10.1113/jphysiol.1969.sp008982.

Gao, W., Li, W., Yan, Y., Yang, R., Zhang, Y., Jin, M., Luo, Z., Xie, L., Ma, Y., Xu, X., Wang, G., Kong, Z., Gao, Y., Li, Y., Ruan, Z., Zheng, J., Ma, D., Wang, Q., 2021. Transcutaneous electrical acupoint stimulation applied in lower limbs decreases the incidence of paralytic ileus after colorectal surgery: a multicenter randomized controlled trial. Surgery 170, 1618–1626. https://doi.org/10.1016/j.surg.2021.08.007.

Israelyan, N., Del Colle, A., Li, Z., Park, Y., Xing, A., Jacobsen, J.P.R., Luna, R.A., Jensen, D.D., Madra, M., Saurman, V., Rahim, R., Latorre, R., Law, K., Carson, W., Bunnett, N.W., Caron, M.G., Margolis, K.G., 2019. Effects of serotonin and slow-release 5-hydroxytryptophan on gastrointestinal motility in a mouse model of depression. Gastroenterology 157, 507–521.e4. https://doi.org/10.1053/j.gastro.2019.04.022.

Jacques, S.L., 2013. Optical properties of biological tissues: a review. Phys. Med. Biol. 58, 37–61. https://doi.org/10.1088/0031-9155/58/11/R37.

Kim, C., 2021. Evolution of advanced miniaturization for active implantable medical devices. In: Nano-Bio- Electronic, Photonic and MEMS Packaging. Springer International Publishing, Cham, pp. 407–415. https://doi.org/10.1007/978-3-030-49991-4_17.

Klapoetke, N.C., Murata, Y., Kim, S.S., Pulver, S.R., Birdsey-Benson, A., Cho, Y.K., Morimoto, T.K., Chuong, A.S., Carpenter, E.J., Tian, Z., Wang, J., Xie, Y., Yan, Z., Zhang, Y., Chow, B.Y., Surek, B., Melkonian, M., Jayaraman, V., Constantine-Paton, M., Wong, G.K.-S., Boyden, E.S., 2014. Independent optical excitation of distinct neural populations. Nat. Methods 11, 338–346. https://doi.org/10.1038/nmeth.2836.

Margolis, K.G., Cryan, J.F., Mayer, E.A., 2021. The microbiota-gut-brain Axis: from motility to mood. Gastroenterology 160, 1486–1501. https://doi.org/10.1053/j.gastro.2020.10.066.

Michels, R., Foschum, F., Kienle, A., 2008. Optical properties of fat emulsions. Opt Express 16, 5907. https://doi.org/10.1364/OE.16.005907.

Million, M., Wang, L., Stenzel-Poore, M.P., Coste, S.C., Yuan, P.Q., Lamy, C., Rivier, J., Buffington, T., Taché, Y., 2007. Enhanced pelvic responses to stressors in female CRF-overexpressing mice. Am. J. Physiol. Regul. Integr. Comp. Physiol. 292, R1429–R1438. https://doi.org/10.1152/ajpregu.00626.2006.

Morais, L.H., Schreiber, H.L., Mazmanian, S.K., 2021. The gut microbiota–brain axis in behaviour and brain disorders. Nat. Rev. Microbiol. 19, 241–255. https://doi.org/10.1038/s41579-020-00460-0.

Patapoutian, A., Peier, A.M., Story, G.M., Viswanath, V., 2003. ThermoTRP channels and beyond: mechanisms of temperature sensation. Nat. Rev. Neurosci. 4, 529–539. https://doi.org/10.1038/nrn1141.

Pope, R.M., Fry, E.S., 1997. Absorption spectrum (380–700 nm) of pure water II Integrating cavity measurements. Appl. Opt. 36, 8710. https://doi.org/10.1364/AO.36.008710.

Reeder, J.T., Xie, Z., Yang, Q., Seo, M.-H., Yan, Y., Deng, Y., Jinkins, K.R., Krishnan, S.R., Liu, C., McKay, S., Patnaude, E., Johnson, A., Zhao, Z., Kim, M.J., Xu, Y., Huang, I., Avila, R., Felicelli, C., Ray, E., Guo, X., Ray, W.Z., Huang, Y., MacEwan, M.R., Rogers, J.A., 2022. Soft, bioresorbable coolers for reversible conduction block of peripheral nerves. Science 377, 109–115. https://doi.org/10.1126/science.abl8532, 1979.

Schneider, C.A., Rasband, W.S., Eliceiri, K.W., 2012. NIH Image to ImageJ: 25 years of image analysis. Nat. Methods 9, 671–675. https://doi.org/10.1038/nmeth.2089.

Spencer, N.J., Bywater, R.A., 2002. Enteric nerve stimulation evokes a premature colonic migrating motor complex in mouse. Neuro Gastroenterol. Motil. 14, 657–665. https://doi.org/10.1046/j.1365-2982.2002.00367.x.

Spencer, N.J., Hibberd, T.J., Travis, L., Wiklendt, L., Costa, M., Hu, H., Brookes, S.J., Wattchow, D.A., Dinning, P.G., Keating, D.J., Sorensen, J., 2018. Identification of a rhythmic firing pattern in the enteric nervous system that generates rhythmic electrical activity in smooth muscle. J. Neurosci. 38, 5507–5522. https://doi.org/10.1523/JNEUROSCI.3489-17.2018.

Spencer, N.J., Hu, H., 2020. Enteric nervous system: sensory transduction, neural circuits and gastrointestinal motility. Nat. Rev. Gastroenterol. Hepatol. 17, 338–351. https://doi.org/10.1038/s41575-020-0271-2.

Spencer, N.J., Kyloh, M., Duffield, M., 2014. Identification of different types of spinal afferent nerve endings that encode noxious and innocuous stimuli in the large intestine using a novel anterograde tracing technique. PLoS One 9, e112466. https://doi.org/10.1371/journal.pone.0112466.

Velasco-Benitez, C., Villamarin, E., Mendez, M., Linero, A., Hungria, G., Saps, M., 2023. Efficacy of transcutaneous posterior tibial nerve stimulation in functional constipation. Eur. J. Pediatr. 182, 1309–1315. https://doi.org/10.1007/s00431-022-04798-w.

Wang, L., Jacques, S.L., Zheng, L., 1995. MCML-Monte Carlo modeling of light transport in multi-layered tissues. Comput. Methods Progr. Biomed. 47, 131–146. https://doi.org/10.1016/0169-2607(95)01640-F.

Wei, H.-J., 2005. Determination of optical properties of normal and adenomatous human colon tissues in vitro using integrating sphere techniques. World J. Gastroenterol. 11, 2413. https://doi.org/10.3748/wjg.v11.i16.2413.

Wu, Y., Wu, M., Vázquez-Guardado, A., Kim, J., Zhang, X., Avila, R., Kim, J.-T., Deng, Y., Yu, Y., Melzer, S., Bai, Y., Yoon, H., Meng, L., Zhang, Y., Guo, H., Hong, L., Kanatzidis, E.E., Haney, C.R., Waters, E.A., Banks, A.R., Hu, Z., Lie, F., Chamorro, L.P., Sabatini, B.L., Huang, Y., Kozorovitskiy, Y., Rogers, J.A., 2022. Wireless multi-lateral optofluidic microsystems for real-time programmable optogenetics and photopharmacology. Nat. Commun. 13, 5571. https://doi.org/10.1038/s41467-022-32947-0.

Yang, Y., Wu, M., Vázquez-Guardado, A., Wegener, A.J., Grajales-Reyes, J.G., Deng, Y., Wang, T., Avila, R., Moreno, J.A., Minkowicz, S., Dumrongprechachan, V., Lee, J., Zhang, S., Legaria, A.A., Ma, Y., Mehta, S., Franklin, D., Hartman, L., Bai, W., Han, M., Zhao, H., Lu, W., Yu, Y., Sheng, X., Banks, A., Yu, X., Donaldson, Z.R., Gereau, R.W., Good, C.H., Xie, Z., Huang, Y., Kozorovitskiy, Y., Rogers, J.A., 2021. Wireless multilateral devices for optogenetic studies of individual and social behaviors. Nat. Neurosci. 24, 1035–1045. https://doi.org/10.1038/s41593-021-00849-x.

Yang, Y., Wu, M., Wegener, A.J., Vázquez-Guardado, A., Efimov, A.I., Lie, F., Wang, T., Ma, Y., Banks, A., Li, Z., Xie, Z., Huang, Y., Good, C.H., Kozorovitskiy, Y., Rogers, J. A., 2022. Preparation and use of wireless reprogrammable multilateral optogenetic devices for behavioral neuroscience. Nat. Protoc. 17, 1073–1096. https://doi.org/10.1038/s41596-021-00672-5.